IMPROVEMENT OF NOISE REDUCTION AND PERFORMANCE FOR A HELICOPTER MODEL ROTOR BLADE BY ACTIVE TWIST ACTUATION

Joëlle BAILLY (joelle.zibi@onera.fr)
Applied Aerodynamics Department, Meudon

Yves DELRIEUX (yves.delrieux@onera.fr)
Numerical Simulations and Acoustics Department, Châtillon

Office National d'Etudes et de Recherches Aéronautiques, France

Abstract

This paper presents the work performed at ONERA in the framework of the WorkPackage 5 of the Friendcopter European project. The objectives of this study consist in the research of optimized active twist laws to improve the performance for advancing flight configurations on the one hand, and reduce BVI noise in descent flight configurations on the other hand, on a BO105-like geometry model rotor with parabolic blade tip. The benefits in terms of power consumption by the main rotor and of noise levels are estimated. Rather limited power benefits are predicted (around 2% for a moderate advancing flight). The power reduction is mainly due to a decrease of the induced power, generated by an adapted distribution of the incidence angle modified by the addition of the active twist angle. A promising reduction of BVI noise (up to -7.4 dBA for a 7deg descent flight) is predicted. This benefit is due to the large effect of the active twist on the downward convection of the wake, which increases the blade-vortex miss-distances and the oblicity of the vortex lattices. The second step of this study is the research of optimized active flap laws on a BO105-like geometry rotor, with the same objectives. The power benefits are also rather limited (no more than -3%). The origin of the power benefit comes from a reduction of the profile power (which depends on the drag model used to account for the flap). The reduction of BVI noise levels is not as satisfactory as for the active twist concept. The indirect servo-flap effect is predominant for the rather soft in torsion studied rotor. The effect of convection is largely reduced due to the aeroelastic response of the rotor.

1. INTRODUCTION

The design of a new helicopter has now to respect environmental constraints which lead to the need in performance improvement, external and cabin noise reduction, and vibration reduction. In order to achieve these improvements, a lot of studies have been performed during the last decades, especially on active rotor blade concepts, such as high harmonic control, active trailing edge, and active twist actuation. For that purpose, appropriate actuation systems are needed. From the experimental point of view, the on-going improvements of the technology on smart materials [1][2] (such as piezo-electric actuators), used for adaptive helicopter rotor blades, allow obtaining significant benefits with such active devices. Various studies have been performed on the simulations of different active devices, such as Individual Blade Control (IBC) [3], Higher Harmonic Control (HHC) [4][5], active twist [6][7], active flap [8], and soft trailing edge [9]. Benefits on BVI noise level, vibration level, and performance [10] have been estimated, using these concepts. More recently, CFD codes have been successfully coupled to comprehensive analysis codes, to improve airload predictions over lifting line theory. These coupled CFD-CSD methods begin to be used to evaluate benefits of active concepts [11].

In this paper, an optimization procedure based on the coupling between the GADO genetic algorithm and the R85 comprehensive rotor code is used to firstly define optimized active twist laws for the performance improvement on the one hand, and the reduction of BVI noise level on the other hand, for a BO-105 like geometry model rotor. Then, optimized active flap laws are compared with these active twist laws. The paper is concluded with a summary of performance and noise improvements predicted for these two concepts, and points out the influence of the aeroelastic response of the studied rotor on these benefits.

©DGLR 2009

2. IMPLEMENTATION OF THE ACTIVE TWIST CONCEPT IN THE COMPUTATIONAL TOOLS

Two approaches can be considered to take into account the effect of the active twist concept in a comprehensive analysis tool:

1- Consider the active twist as the resultant of an external couple applied on the blade, which is superimposed on the aerodynamic moment [12];
2- Consider the active twist as an additional geometric twist for the evaluation of the geometric total incidence angle.

The first approach has the advantage to directly provide the required energy to deform the blade, which is very interesting from the experimental point of view. Nevertheless, the active twist required to reach the objective is only a part of the simulation.
The second approach has the advantage of considering the harmonic components of the active twist as input data of the simulations. Furthermore, this approach is much more compatible than the first one for the control of such a device. These reasons lead to the choice of the implementation of this second approach in the aero-elastic and the free-wake computational tools used by ONERA during the optimization process.

2.1 Description of the computational tools

The R85 code (developed by Eurocopter [13]) is an aeroelastic code used to compute rotor trim, aerodynamic performance, and vibration properties of the rotor. The aerodynamic modelling is based on the lifting line theory. At each azimuth and for each section, an angle of attack and a sectional Mach number are computed and used to read aerodynamic coefficients in 2D polars. The wake model is computed by the METAR code [14], and is defined by a prescribed helicoidal geometry described by vortex lattices. A coupling between R85 and METAR is made until convergence is reached on induced velocities at the rotor disk level. The flexibility of the blades is also taken into account by solving the Lagrange equations.

A specific procedure has been developed to split the total power consumed by the main rotor as the sum of different contributions:

(1) *Total Power = Induced Power + Profile Power + Fuselage Power.*

It is reminded that the induced power generates the global lift. The profile power compensates the drag of the blades. The fuselage power compensates the global drag of the helicopter. Each of these terms is obtained by adding the elementary terms on each blade element. This decomposition also allows visualizing and analyzing the evolutions of the different power terms on the rotor disk.

The prescribed wake geometry obtained by R85/METAR is then distorted by using a free wake analysis code, MESIR [15]. In this code, a lifting line method similar to that in R85/METAR is used. The blade motion calculated in R85 is given to the MESIR code. In the wake deformation process, the whole wake structure is distorted, and wake geometry iterations are continued until circulation convergence is achieved after a few iterations.
An intermediate step between wake geometry and blade pressure calculation is introduced using the MENTHE code [16]. During the roll-up process of the vortices, MENTHE identifies the parts of vortex sheets that the MESIR code calculated as having sufficiently strong intensity to roll-up. These rolled sheet regions constitute interacting vortices.
Blade pressure distribution is then calculated by the unsteady singularity method, ARHIS [17]. This code assumes that the flow around the rotor is inviscid and incompressible. It performs 2D-by-slices computations. Subsonic compressibility effects are included by means of Prandtl-Glauert corrections combined with a local thickening of the airfoil. In addition, finite span effects are introduced through an elliptic-type correction of the pressure coefficients. The interacting vortices are modelled as freely convecting and deforming clouds of vortex elements. The main advantage of this method is the ability to take into account the vortex deformation during strong blade-vortex interactions.
The noise radiation is computed by the PARIS code [18], using pressure distribution computed by ARHIS. The PARIS code is based on the Ffowcs Williams-Hawkings equation and predicts the loading and thickness noise. It uses a time domain formulation. An efficient spanwise interpolation method is implemented. It identifies the BVI impulsive events on the signatures generated by each individual blade section.

2.2 Description of the active twist model

The active twist functionality is implemented in the two codes used at ONERA: R85, the comprehensive aeroelastic rotor code (in the same way for the aerodynamic, acoustic and dynamic computations in forward flight) and

MESIR, the free wake code (used for the acoustic computations). In each case, the active twist laws are written as follows:

$$(2)\ \Delta\tau(\Psi) = \tau_0 + \sum_{i=1}^{5} \tau_{ic}\cos(i\Psi) + \tau_{is}\sin(i\Psi)$$

The input parameters in R85 and MESIR codes for active twist computations are then: spanwise extension of active twist (Rstart, Rend), τ_0, τ_{ic}, τ_{is} Up to 5 harmonics have been considered, with respect to the specifications of the mechanical designers of the active twist device. Since these devices are expected to give an over-twist rate along the blade span where the active twist is effective, it has been chosen to pilot the active twist from the last active twist section (Rend) and to linearly interpolate the active twist deflection on the inner spanwise location as illustrated in Figure 1.

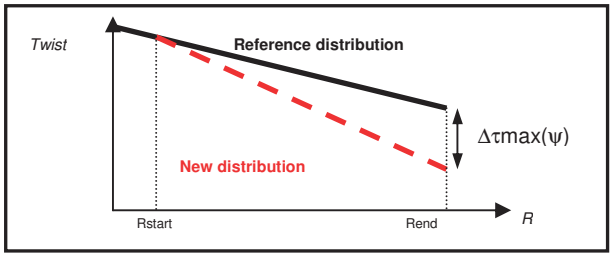

Figure 1: Scheme of the active twist deflection model

In the R85 code, the active twist deflection $\Delta\tau$ is added to the local twist τ, the local pitch angle θ, and the local elastic torsional deformation *torsion* to give the geometrical angle-of-attack defined as:

(3) $\alpha = \theta + \tau + \boldsymbol{\Delta\tau} + torsion$

Active twist is taken into account in MESIR in the same way as in R85, through the local angle-of-attack computations.

2.3 Description of the optimization chain

The optimization procedure MORPHIA [19] has been developed at ONERA to optimize the rotor blade shapes with the possibility to simultaneously take into account hover flight performance and forward flight performance. It is built around two optimization algorithms, a gradient-based method CONMIN [20], and a genetic algorithm GADO [21], which have been coupled with the *elsA* 3D Navier-Stokes solver (used for hover) and the R85 or HOST comprehensive rotor codes (used for forward flight), as shown in Figure 2.

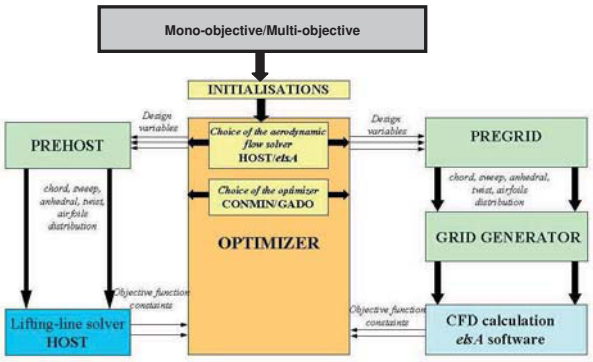

Figure 2: Scheme of the MORPHIA optimization chain

In the framework of this study, it has been chosen to use the genetic algorithm GADO coupled with the aeroelastic code R85. GADO is a genetic algorithm especially devoted to shape optimization. It combines basic techniques of the genetic algorithms with a progressive research strategy. This latter consists, at the beginning of the research of the optimum, in privileging the exploration of the research domain, and then in progressively focussing on the precise location of the global optimum.

The selection strategy corresponds to the criteria applied to choose the individuals who are addressed to become the parents of a new individual. This selection favours the individuals with best performances. GADO assigns to each individual a weight directly linked to its position in the classification by merit. The probability of this individual to be selected is proportional to this weight. Two selection operators are used to generate a new individual: crossing and mutation. Then, a filtering module is applied. The new individual is compared to the existing evaluated individuals kept in memory. If it is too close to individuals with a bad performance, it is rejected before its evaluation saving CPU time. Finally, the diversity module allows a sufficient diversity of the population to avoid a premature convergence.

The choice of GADO as an optimizer instead of CONMIN optimizer has been made to ensure, as far as possible, the detection of the global optimum.

2.4 Definition of the reference model rotor and test cases

The definition of the reference model rotor results from a compromise between the strong demands of the partners of the FRIENDCOPTER-WP5 project (in which this study has been performed) for a recent blade

©DGLR 2009

geometry, and the need to validate tools preferably on a blade that most of the partners are familiar with. The reference model rotor is a modified BO-105 rotor, composed of 4 blades, with a rectangular shape up to 0.9516R, followed by a parabolic tip (similar to the ONERA 7AD model rotor). The blade is equipped with the NACA23012 airfoil (between the blade root 0.22R and 0.75R), and the OA209 airfoil (between 0.9R and the blade tip 1R). Interpolated airfoils are used between 0.75R and 0.9R. The rotor radius is equal to 2m, and the chord to 0.121m. The aerodynamic twist is equal to -8°/R, and is 0° at 0.7R. The pitch axis is located on the quarter line. This reference rotor is named NMR (New Model Rotor).
The structural characteristics of this reference rotor, taking into account the technological constraints of the piezo-electric actuators for active twist device have been defined by DLR, and a model rotor blade has been designed and manufactured [22].
The potential improvement in rotor aerodynamic performance and the reduction in external noise due to the implementation of an active rotor with actuation technology are evaluated on different typical flight configurations.

For the performance evaluations, the following forward flight configurations are chosen:
μ=0.307, Vh=130kts, $M_{\Omega R}$=0.640, C_T/σ=0.06, 0.075, 0.085
For the noise computations, different descent flight configurations are chosen, corresponding to different descent angles:
μ=0.152, Vh=64.34kts, $M_{\Omega R}$=0.640, C_T/σ=0.056, α_d varying from 0° (level flight) to 10° each 2°, and 7°.
Target benefits to be achieved by the active rotor technology (with respect to the passive rotor) have been specified:

- A gain of 5% of the power consumed by the main rotor;
- A reduction of -5dB of BVI noise for an approach flight configuration.

3. ANALYSIS OF THE AERODYNAMIC OPTIMIZATION RESULTS

3.1 Numerical optimization data

The active twist area on the NMR rotor is defined on the rectangular part of the blade, i.e. between Rstart/R=0.22 and Rend/R=0.9516. The objective function is the minimization of the total power consumed by the main rotor. The search for the optimized active twist laws has been adapted for each value of the rotor thrust coefficient (defined in §2.4). Taking into account 10 optimization variables, the number of GADO individuals is set at 100, and the number of evaluations at 3000.
The maximum twist amplitude at the last active section is set at ±2°. The side constraints on each of the optimization variables are set at the same values.

3.2 Definition of optimized control laws

The evolutions of the optimized active twist laws obtained for each rotor thrust coefficient are plotted in Figure 3. These laws have rather similar shapes for the three configurations, with especially an important variation between 120° and 200°, and contain up to 4/rev and 5/rev harmonic components.

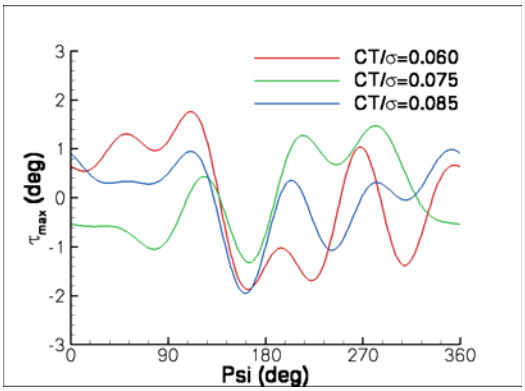

Figure 3: Evolutions of active twist laws optimized for performance (NMR rotor)

3.3 Benefit calculations

The convergence history of the objective function and the decision variables during the GADO process has been checked for the three configurations. Satisfactory level of convergence on these variables has been obtained.
For the three test cases, some benefits on the total power are obtained (even though they are rather limited, varying from -0.3 to -2.3%), as shown in Figure 4.

©DGLR 2009

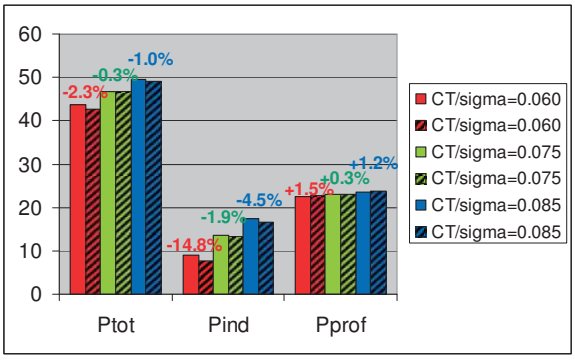

Figure 4: Predicted power terms (in kW) and benefit power calculations for inactive NMR (plain) and NMR with active twist (hachured)

Thanks to the procedure which splits the total power, it can be seen for each test case, that the use of the optimized active twist laws allows a more important decrease of the induced power than the increase of the profile power. These evolutions are shown in Figure 5, which represents the surfacic distribution on the rotor disk of the difference of the induced and the profile powers between the active and the inactive NMR rotor, for the lowest rotor thrust coefficient (C_T/σ=0.060). The blue areas represent the zones where a benefit in the power is predicted, the red ones where an increase of power is estimated. Two major areas where the induced power is increased by applying the active twist law can be identified near the blade tip: between 90° and 110° of azimuth on the advancing side, and between 240° and 270° on the retreating side. These areas correspond to the maximal added values of the active twist, which increase the local incidence (Figure 7), and so the local lift (Figure 6), and so the induced power. A large region of the rotor disk where the optimized active twist law leads to a decrease of the induced power can be observed (blue zone). The influence of this area is predominant with respect to the zone where a deficit of induced power is predicted, as the global benefit of induced power is about -15%. For instance, at the azimuth of 160° where the active twist angle is minimal, the local incidence is decreased (Figure 7), which leads to a lower value of the lift coefficient (Figure 6), which explains the reduced value of the induced power. Concerning the distribution of the profile power, two main regions where the actuation of the active twist increases this component of the power are at the blade tip: on the advancing side between 90° and 180°, and on the retreating side between 240° and 270°. These areas correspond to an added positive value of the active twist angle, which makes increase the local incidence (Figure 7), and so the local lift (Figure 6) (as explained above), and so the local drag. There is a direct link between the drag coefficient and the profile power distributions (Figure 5 and Figure 6). The areas where the increase of profile power is predicted are predominant with respect to the rest of the rotor disk where the difference between the active and the inactive rotors is close to 0. This explains the global increase of this component in the power evaluation.

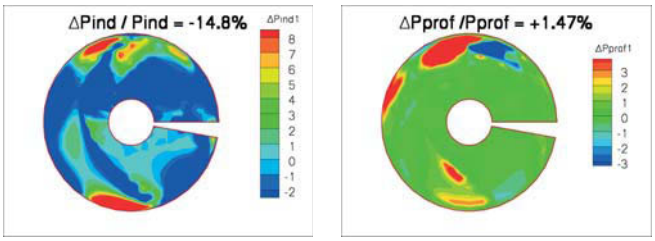

Figure 5: Surfacic distribution of the difference (NMR with active twist - inactive NMR) on the induced power (left) and the profile power (right) - C_T/σ=0.06, Vh=130 kts

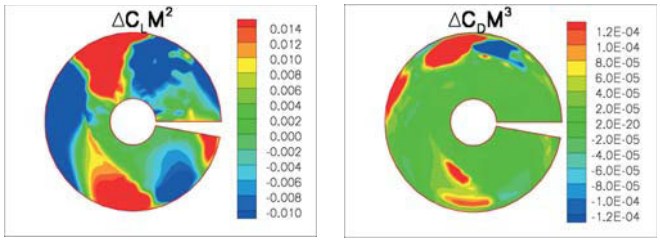

Figure 6: Surfacic distribution of the difference (NMR with active twist - inactive NMR) on the lift coefficient (left) and drag coefficient (right) - C_T/σ=0.06, Vh=130 kts

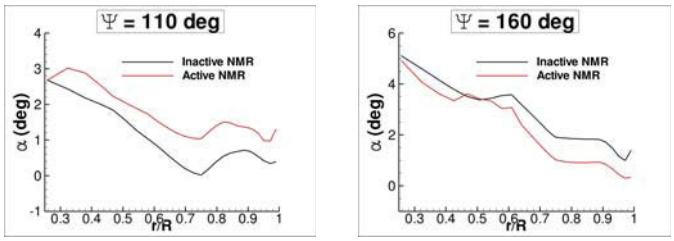

Figure 7: Effect of active twist on the geometric incidence angle for the NMR rotor - C_T/σ=0.06, Vh=130 kts

To conclude, the gains on the total power predicted with the optimized active twist laws on three advancing configurations are rather limited, varying from -0.3 to -2.3% (these gains do not reach the targets defined in the Friendcopter

©DGLR 2009

project). The origin of the power benefit comes from a decrease of the induced power. The use of the optimized active laws directly modifies the incidence angle, and allows a better distribution of the loads on the rotor disk.

4. ANALYSIS OF THE ACOUSTIC OPTIMIZATION RESULTS

4.1 Numerical optimization data

Similarly to the procedure explained in §3, active twist laws are optimized to reduce the BVI noise, using the GADO optimizer coupled with the R85 aero-elastic code. The objective function is the maximization of the induced velocity, near the blade tip ($0.7 \leq r/R \leq 0.9$), on the advancing side ($70° \leq \psi \leq 110°$). This objective function has been chosen to obtain a faster downward convection of the wake. The active area is also defined in the rectangular part of blade (Rstart/R=0.22 and Rend/R=0.9516). The optimization variables are the sine terms from 1 to 5 per-rev of the harmonic components of the active twist. The number of GADO individuals is set at 100, and the number of evaluations at 3000. The maximum blade amplitude at the last active section is set at ±2°. The side constraints on each optimization variables are set at the same values.

4.2 Definition of optimized control laws

The evolutions of the optimized control laws obtained for BVI noise reduction, for each descent angles, are represented in Figure 8.

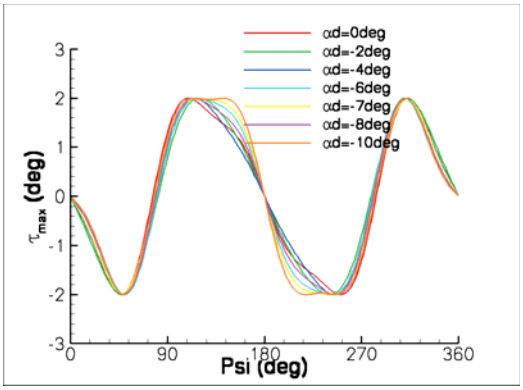

Figure 8: Evolutions of active twist laws optimized for BVI noise

These laws have very similar shapes, with a predominant 2/rev harmonic component. As the descent angle grows, the maximum (+2°) and the minimum (-2°) active twist values are maintained on larger azimuthal areas (respectively around 110° and 250°).

The distributions of the induced velocities fields, computed by the R85 code, for the angle of descent α_d of -7° are compared for the inactive and the active NMR rotor (Figure 9). It can clearly be seen that the optimized control law provides a higher value of the averaged velocity in the selected area of the rotor disk (+156% for α_d=-7°). It has been checked that the same trend is obtained for the other descent flight configurations.

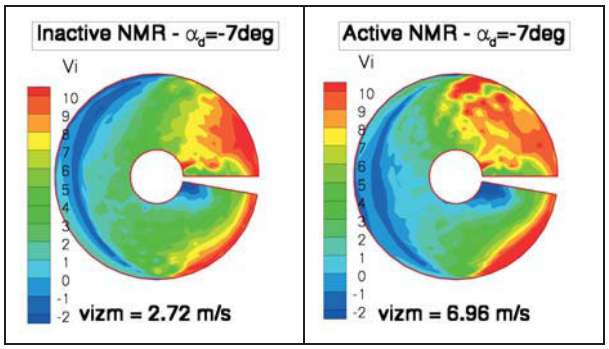

Figure 9: Distribution of the induced velocity fields for the inactive NMR (left), and the NMR with active twist (right) - α_d=-7°

4.3 Benefit calculations

The comparison of the maximum noise level on a carpet located 2.7m underneath the rotor versus the descent angle between the inactive and the active rotors is plotted in Figure 10. The levels are expressed in dBA filtered in the frequency range comprised between the 6th and 40th harmonics of the blade passage frequency. This range corresponds to the frequency domain where BVI noise dominates.

Thanks to the optimized laws, important noise reduction are obtained in a large range of descent angle around 6° and 7°, which corresponds to the maximum noise emission for the inactive rotor.

©DGLR 2009

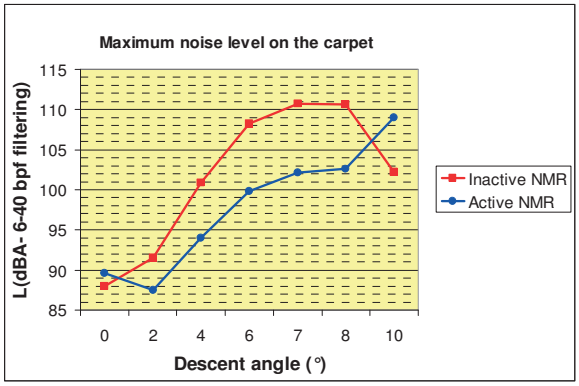

Figure 10: Effect of active twist on the maximum noise levels for the NMR rotor

The highest noise reduction is obtained at the angle of descent of -7°, with a decrease of the BVI noise level of -7.4 dBA. The noise contours obtained on the carpet for α_d=-7° are shown in Figure 11 for the inactive and the active NMR rotors.

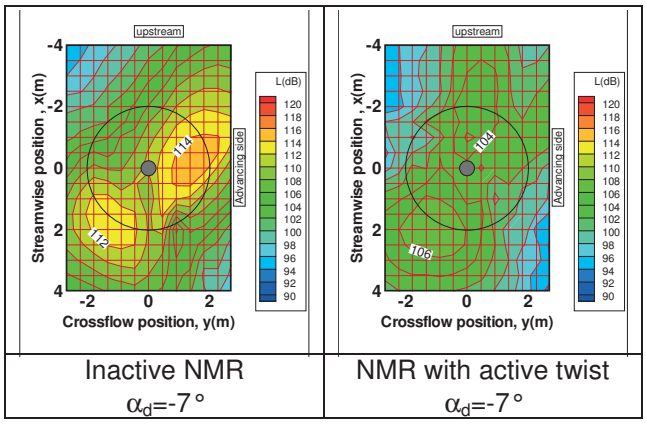

Figure 11: Computed noise contours for the inactive NMR (left) and NMR with active twist (right) – α_d=-7°

For this descent angle, the noisiest areas have been dramatically reduced both on the advancing and on the retreating sides of the blade, thanks to the application of the optimized active twist laws. This noise reduction can easily be explained by the huge modification of the blade vortex miss-distances, as shown in Figure 12.

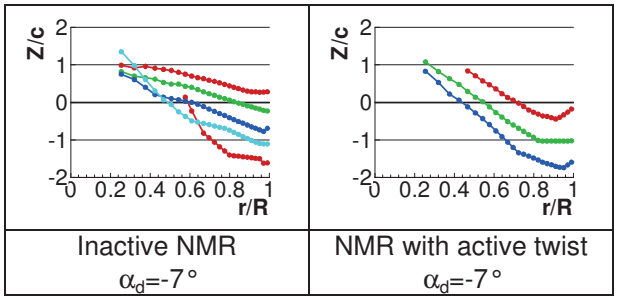

Figure 12: Blade-vortex miss-distances of the inactive NMR (left) and the NMR with active twist (right) - α_d=-7°

The optimized active twist laws are effective to increase the blade-vortex miss-distances in the noisy configurations. Figure 12 clearly shows the effect of the downward convection of the wake provided by the application of the active twist law. For instance, the green lattice has moved by about 1 chord length below the blade, which can be the origin of a decrease of about 5 dB of the noise level. Furthermore, the lattices of the active rotor are much more oblique than the ones generated by the inactive rotor. The interactions with the blade are located more inboard and at higher blade azimuths. All these modifications of the wake can explain the important reduction of the BVI noise level for the 7° descent flight configuration. Similar effects of the optimized active twist laws are observed for the other descent angles, between -2° and -8°. For the descent angle where the BVI phenomenon is less pronounced (level flight at α_d=0°, and steep descent angle at α_d=-10°), the application of the active twist laws does not allow to reduce the BVI noise level. Other strategies have to be found to reduce the noise emission for these flight conditions. For instance, at -10°, it was tried to decrease the BVI noise on the advancing side by decreasing the averaged induced velocities, near the blade tip, on the advancing side of the blade. This strategy is shown efficient on the advancing blade side but a penalty is predicted on the retreating side.

The active twist device, applied on the NMR model rotor, seems to be very efficient to reduce the BVI noise, especially thanks to the predicted modification of the downward convection of the wake. The target of the Friendcopter project is theoretically reached.

©DGLR 2009

5. COMPARISON WITH THE ACTIVE FLAP CONCEPT

Another well-known active concept for performance improvement and noise reduction consists in setting an active flap device at the trailing edge of the blade. Thanks to new technologies, this concept has been increasingly studied and applied.

5.1 Description of the active flap model

Two ways for modelling the aerodynamic effect of a trailing edge flap in a comprehensive code can be considered:

1- semi-empirical laws
2- computation of airfoil polars using 2D (or 3D) CFD codes, for different angles of deflections.

In the framework of this study, it has been chosen to introduce semi-empirical laws in the R85 aero-elastic code. During previous studies performed at ONERA on the active flap [23], it has been shown that, in a first approximation, an asymptotic development of first order with respect to the angle of deflection δ gives the relation between the aerodynamic coefficients of the deformed airfoils and the aerodynamic coefficients without blade deflection. Linear relations between the deflected and initial lift coefficient Cl and pitching moment Cm can be used. For the drag coefficient Cd, this linear relation can not be applied. A translation proportional to the angle of deflection and an additional penalty have to be taken into account. Furthermore, it has been shown that the shapes of the polars of the lift and pitching moment show a quasi-linear relation between these coefficients and the angle of deflection δ, for all values of Mach number M, and angle of incidence α. It means that the values of the gradients $\partial C_L/\partial\delta$ and $\partial C_M/\partial\delta$ only depend on the chordwise extension of the active area of the blade *cv/c*. For a given value of *cv/c*, the following semi-empirical laws are used (δ given in degrees and positive for a downward deflection):

$$(4)\quad C_{L\,flap} = C_{L\,no\_flap} + C_1(cv/c)\times\delta$$

$$(5)\quad C_{M\,flap} = C_{M\,no\_flap} - C_2(cv/c)\times\delta$$

$$(6)\quad C_{D\,flap}(M,\alpha,\delta) = C_{D\,no\_flap}(M,(\alpha - C_3\times\delta)) + C_4\times\delta$$

where C_1 and C_2 are constants depending only on *cv/c*, and C_3 and C_4 are constants which do not depend on the Mach number, the incidence angle and the angle of deflection.

As for the active twist model, the active flap laws are introduced in the R85 aero-elastic code and MESIR free-wake code in harmonic form, with a maximum of 5 components:

$$(7)\quad \delta(\Psi) = \delta_0 + \sum_{i=1}^{5} \delta_{ic}\cos(i\psi) + \delta_{is}\sin(i\psi)$$

applied all along the spanwise extension of the active flap.

In the Friendcopter specifications, the active area is located between 0.6 and 1 rotor radius, and the chordwise extension is equal to 0.20 chord length.

5.2 Definitions of the reference model rotor and test cases

In order to avoid an active flap area in that parabolic blade tip of the NMR rotor, it was decided to evaluate the active flap concept on the BO105-like geometry rotor, named BMR. This rotor has four rectangular blades, equipped with the NACA23012 airfoil. The rotor radius is equal to 2m, and the chord to 0.121m. The aerodynamic twist is equal to -8°/R.

For the performance evaluations, the following forward flight configurations are considered:
1- Vh=130kts, C_T/σ=0.06, μ=0.307, $M_{\Omega R}$=0.640
2- Vh=145kts, C_T/σ=0.08, μ=0.343, $M_{\Omega R}$=0.640
3- Vh=160kts, C_T/σ=0.06, μ=0.378, $M_{\Omega R}$=0.640
The first test case is common with the first one studied for the active twist concept (§2.4).
For the noise computations, the same descent flight configurations as those chosen for the active twist concept (§2.4) are considered.

5.3 Analysis of the aerodynamic optimization results

5.3.1 Numerical optimization data

The same optimization tool and the same characteristics of the optimization procedure (objective function, design variables, constraints) as the ones used for the active twist concept (§3.1) are considered for the active flap concept.

5.3.2 Definition of optimized laws

The evolutions of the optimized active flap laws obtained for each test case are plotted in Figure 13. These laws have rather similar shapes, and contain up to 4/rev and 5/rev harmonic components.

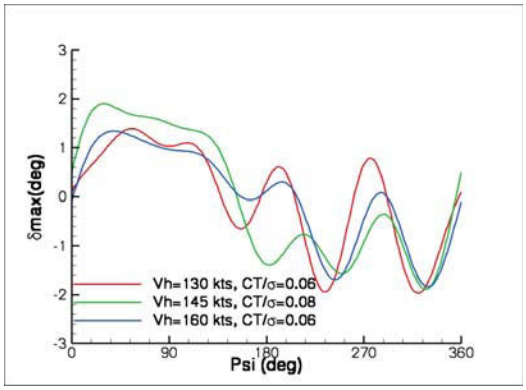

Figure 13: Evolutions of active flap laws optimized for performance (BMR rotor)

It can be noticed, in Figure 14 that for the first test case (common with the active twist study), the evolutions of the optimized active twist law and active flap law are rather close, in terms of amplitude and phase.

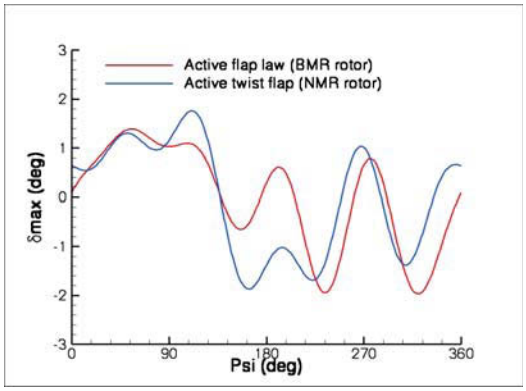

Figure 14: Comparison of active twist (NMR rotor) and active flap (BMR rotor) optimized laws for performance - C_T/σ =0.06, Vh=130 kts

5.3.3 Benefit calculations

It is reminded that the total power is the sum of the induced power, the profile power, and the fuselage power. The power required for the actuation of the flap is not taken into account in these computations.

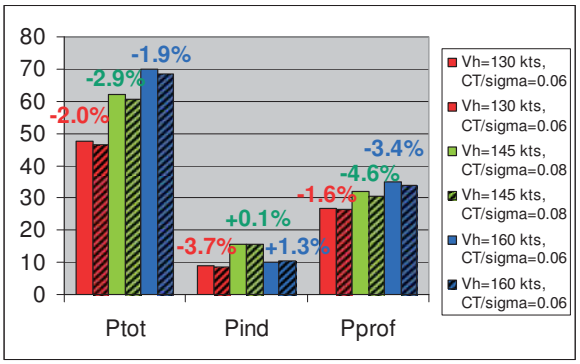

Figure 15: Predicted power terms (in kW) and benefit power calculations for inactive BMR (plain) and BMR with active flap (hachured)

As shown in Figure 15, power benefit obtained with the active flap concept varies from 2 to 3%, for the three flight configurations. For the first test case, this benefit is of same order as the one obtained with the active twist law. The major contribution of the power benefits obtained with the active flap concept comes from the reduction of the profile power (especially for the second and third test cases). To explain these trends, it is interesting to analyse in Figure 16, the evolution of the aerodynamic coefficients of the BMR rotor, without and with the active flap law, for the first test case.

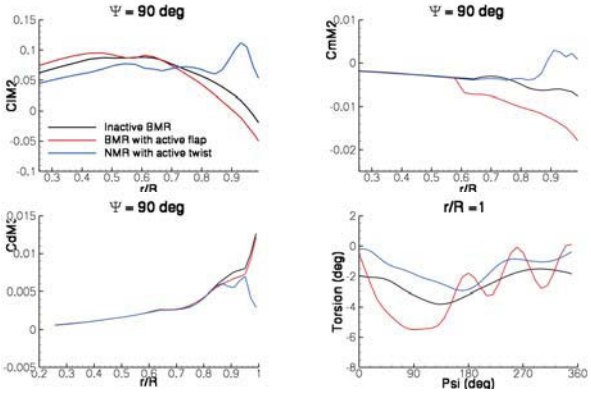

Figure 16: Effect of active flap (BMR) and active twist (NMR) laws on the aerodynamic coefficients (ψ=90°) and on the torsion deformation (r/R=1) – C_T/σ=0.06, Vh=130 kts

The effect of the active flap applied on the BMR rotor is clearly shown by the sudden decrease of the moment coefficient, at the first active section Rstart/R=0.60, which is directly linked with the downward deflection of the flap at 90° of azimuth. Obviously, this evolution does not appear with the active twist law applied on the NMR rotor. The increase of pitching moment of

©DGLR 2009

the NMR is directly due to the parabolic blade tip.
As the BMR rotor is rather soft in torsion (value of the torsion mode close to 4/rev), the aero-elastic response of the BMR provided by the active flap leads to an increase of the amplitude and of the harmonic content of the torsion deformation at the blade tip. In comparison, the torsion deformation of the NMR rotor with the active twist is very similar to the one of the inactive BMR (with a shift of the static value). This means that the optimized active twist has almost no influence on the torsion deformation of the NMR rotor.
This aero-elastic response of the BMR rotor with the active flap has a direct impact on the lift, which is decreased from the beginning of the flap, r/R=0.6. Finally, a decrease of the drag coefficient can be observed from r/R=0.8, for the BMR with active flap, which explains the major benefit obtained on the profile power. It can be concluded that the indirect servo effect of moment is predominant with the active flap law applied on the BMR rotor, which is due to the torsion softness of this rotor. Furthermore, the gains with the active flap are certainly highly sensitive to the drag model used to account for the flap.
The comparison with the active twist law applied on the NMR rotor shows that similar power benefits are estimated for the first test case, for both devices, but for different reasons. It can be reminded that the major reason of the power benefit by the active twist comes from a reduction of the induced power.

5.4 Analysis of the acoustic optimization results

5.4.1 Numerical optimization data

The same optimization tool and the same characteristics of the optimization procedure (objective function, decision variables, constraints) as the ones used for the active twist concept (§4.1) are considered for the active flap concept.

5.4.2 Definition of optimized laws

The optimized active flap laws, obtained for each angle of descent, are plotted in Figure 17.

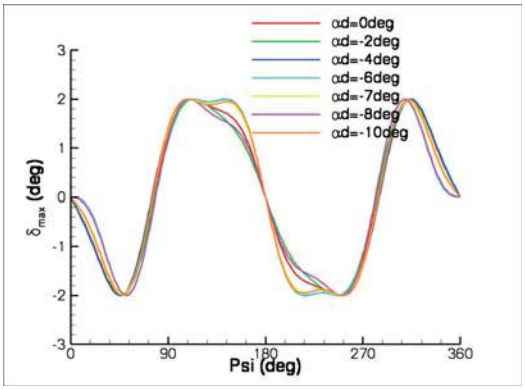

Figure 17: Evolutions of active flap laws optimized for BVI noise (BMR rotor)

These laws mainly contain 2/rev harmonic components, for each value of the descent angle. The spreading of the minimum and maximum values is more or less pronounced with respect to the descent configuration.
It is also interesting to remark, as shown in Figure 18, that the optimized active twist and active flap laws are very similar, for the angle of descent of -7°. This can be explained by the fact that the same optimization procedure (R85 coupled with GADO) has been used, and that the same objective function and design variables have been chosen.

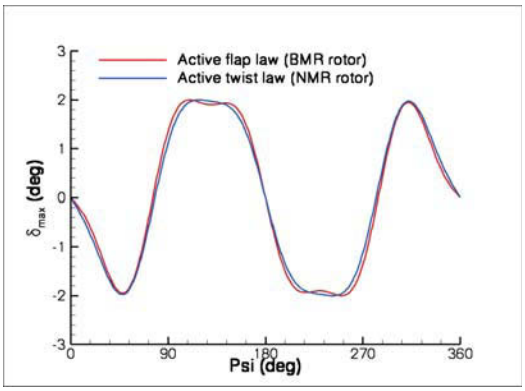

Figure 18: Comparison of active twist (NMR) and active flap (BMR) laws optimized for BVI noise - α_d=-7°

The induced velocity fields are computed by the R85 code, for the inactive and activated flap BMR rotors, for the angle of descent of -7°, as shown in Figure 19.

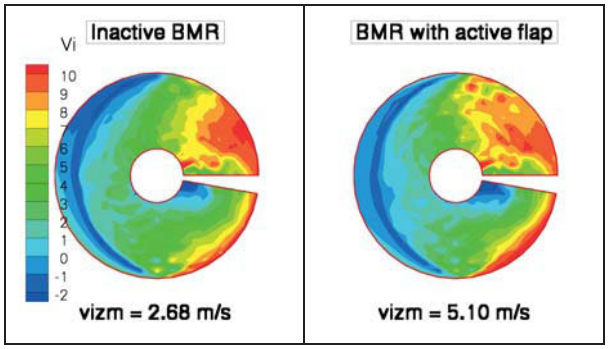

Figure 19: Distribution of the induced velocity fields for the inactive BMR (left) and the BMR with active flap (right) - α_d=-7°

The optimized active flap law provides higher value of the averaged induced velocity in the selected area of the rotor disk, of about +90% for the -7° descent angle. It can be noticed that this increase in the objective function is smaller than the one obtained with the active twist law. This trend is observed for all descent angles. Furthermore, it has also been checked that the application on the BMR rotor of the active twist law defined for the NMR rotor allows an increase of about +161% of the averaged induced velocity. This means that the active flap device has a less pronounced influence on the convection of the wake than the active twist device for the BMR rotor.
The evolution of the aerodynamic coefficients at the azimuth of vortex emission (130°) and the torsion deformation at the blade tip, for the angle of descent of -7°, are respectively plotted in Figure 20.

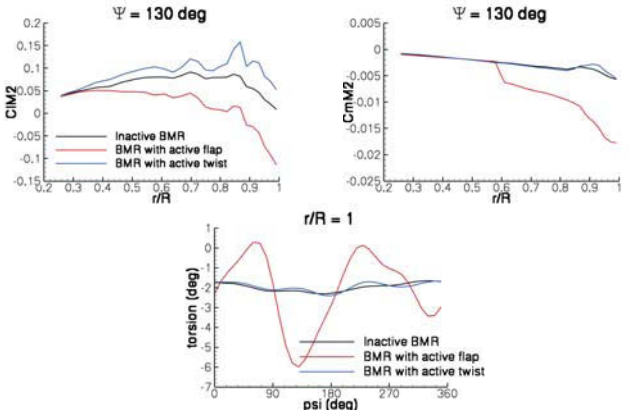

Figure 20: Effect of active flap and active twist laws on the aerodynamic coefficients (ψ=130°) and on the torsion deformation (r/R=1) for the BMR rotor - α_d=-7°

The predominant effect of the flap on the BMR rotor can be clearly seen. At the azimuth of 130°, the downwards flap deflection (δ_{max}=2°) leads to an important nose-down pitching moment, which begins at the first active flap section (Rstart/R=0.6). Due to the softness in torsion of the BMR rotor (value of the torsion mode close to 4/rev), the response in torsion with the active flap provides a very high amplitude of torsion deformation (around 7°). This has a direct impact on the lift, which is decreased, and will explain the noise levels evaluations presented below.
The active twist concept gives very different trends: a higher value of the lift coefficient all along the blade span, and a very small influence on the moment coefficient and torsion deformation.

5.4.3 Benefit calculations

The maximum noise levels on the carpet obtained for the inactive BMR and the BMR with active flap are presented in Figure 21.

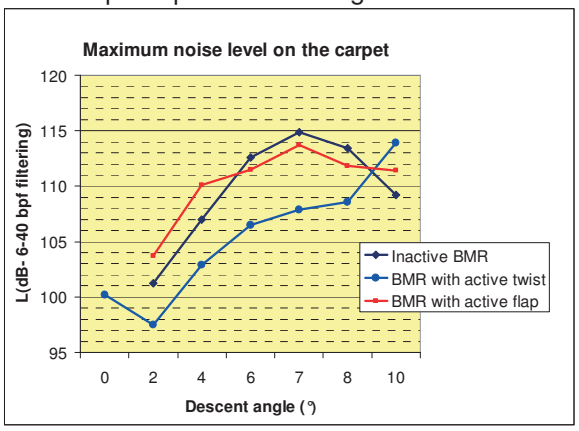

Figure 21: Effect of active flap and active twist laws on the maximum noise levels for the BMR rotor

It can be noticed that for an angle of descent varying from -6° to -8°, a small decrease of maximum noise level is obtained (no more than 1.6 dB). For the small angles of descent (varying from -2° and -4°), a penalty on noise level (up to +3dB) can be reached. On the contrary, as for the NMR rotor, much higher noise levels benefits are predicted with the active twist device (except for the level flight (α_d=0°), and very high descent angle of 10°).
These small noise benefits obtained with the active flap concept can be explained by the blade-vortex miss-distances, for instance for α_d=-7°, in Figure 22.

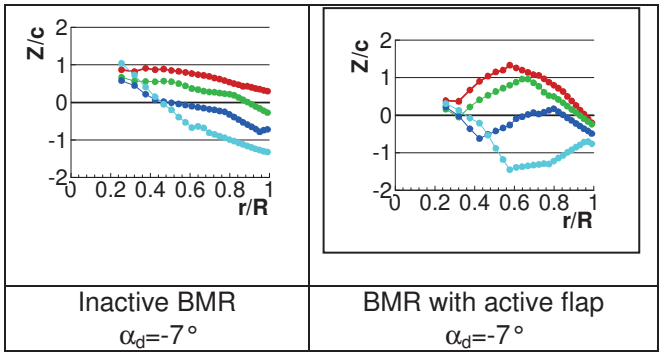

Inactive BMR α_d=-7°	BMR with active flap α_d=-7°

Figure 22: Blade-vortex miss-distances of the inactive BMR (left) and the BMR with active flap (right) - α_d=-7°

With the active flap calculations, the vortices remain in the vicinity of the blade tip and the modification of the wake geometry results only a small noise reduction. Contrary to the active twist concept, the active flap concept does not generate on the BMR rotor as large downward deflection of the wake (Figure 12), which allowed an important noise level reduction.
The effect of the convection is largely reduced by the aeroelastic response of the BMR rotor (very high amplitude of torsion deformation, decrease of the lift) due to its softness.
To conclude, for the BMR rotor, the active flap concept seems to be not as well adapted as the active twist concept to obtain (as shown by the simulations) significant levels of BVI noise reduction.

6. CONCLUDING REMARKS

This paper presented the work performed at ONERA in the framework of the Workpackage 5 of the Friendcopter European project. The first objective of this study was to determine optimized active twist laws to improve the performance in advancing flight configurations on the one hand, and to reduce BVI noise in descent flight configurations on the other hand, for a BO105-like geometry model rotor.
The active twist model was considered as an additional term of the angle of incidence.
Rather limited gains on performance were predicted (around 2%), mainly due to a decrease of the induced power, linked to a better repartition of the aerodynamic loads on the rotor disk. The acoustic computations provided a promising BVI noise level reduction (up to -7.4 dBA), thanks to the large effect of the active twist laws on the downward convection of the wake.
The second objective was to compare these gains with the active flap concept. The active flap effect was modelled by modifying the 2D look-up tables, based on semi-empirical laws. Power gains of about 3% are predicted, but the origin of this benefit mainly comes from a reduction of the profile power (which depends on the drag model used to account for the flap). The reduction of BVI noise level is not as satisfactory as with the active twist concept. Due to the softness of the studied model rotor, the indirect servo-flap effect is predominant. The effect of the active flap on the convection of the wake is largely reduced due to the aeroelastic response of the rotor.
These results could be used in further studies in the definition and specification of active twist device for wind tunnel tests.

7. ACKNOWLEGMENTS

This research is funded in part by the EU in the sixth framework programme as part of the Friendcopter project. The authors would specially like to thank the different partners (DLR, ECD, AW, and NLR) involved in the benefits computations for their active collaboration.

8. REFERENCES

[1] Chopra I., "*Review of State of Art of Smart Structures and Integrated Systems*", AIAA Journal, Vol. 40, No. 11, November 2002, pp. 2145-2187
[2] Chopra I., *"Status of Application of Smart Structures Technology to Rotorcraft Systems"*, Journal of the American Helicopter Society, Vol. 45, No. 4, October 2000, pp. 228-252
[3] Jacklin S.A., Blaas A., Teves D., Kube R., *"Reduction of Helicopter BVI Noise, Vibration, and Power Consumption through Individual Blade Control"*, 51st American Helicopter Society Forum, Fort Worth, TX, May 9-11, 1995
[4] van der Wall B. G., Burley C. L., Yu Y., Richard H., Pengel K., Beaumier P., *"The HART II Test – Measurement of Helicopter Rotor Wakes"*, Aerospace Science and Technology, Vol. 8, (4), 2004
[5] Cheng R.P., Celi R., *"Optimum Two-Per-Revolution Inputs for Improved Rotor Performance"*, Journal of Aircraft. Vol. 42, (6), November-December 2005, pp. 1409-1417
[6] Thepvongs S., Cesnik C., *"Numerical Investigation of Integral Twist Actuation for BVI Noise Reduction"*, 62nd American Helicopter Society Forum, Phoenix, Arizona, May 9-11, 2006

©DGLR 2009

[7] Wilbur M.L., Yeager W.T. Jr, Sekula M.K., *"Further Examination of the Vibratory Loads Reduction Results from the NASA/Army/MIT Active Twist Rotor Test"*, 58th American Helicopter Society Forum, Montreal, Canada, June 11-13, 2002
[8] Nitzsche F., Feszty D., Waechter D., Bianchi E., Voutsinas S., Gennaretti M., Coppotelli G., Ghiringhelli G.L.,"*The SHARCS Project: Smart Hybrid Active Rotor Control System for Noise and Vibration Attenuation of Helicopter Rotor Blades*", 31st European Rotorcraft Forum, Florence, Italy, September 13-15, 2005
[9] Altmikus A., Dummel A., Heger R., Schimke D.,"*Actively Controlled Rotor: Aerodynamic and Acoustic Benefit for the Helicopter Today and Tomorrow*", 34th European Rotorcraft Forum, Liverpool, United Kingdom, September 16-18, 2008
[10] Yeo H., *"Assessment of Active Controls for Rotor Performance Enhancement"*, 62nd American Helicopter Society Forum, Phoenix, Arizona, May 9-11, 2006
[11] Jain R., Szema K.-Y., Munipalli R., *"CFD-CSD Analysis of active Control of Helicopter Rotor for Performance Improvement "*, 65th American Helicopter Society Forum, Grapevine, Texas, May 27-29, 2009
[12] Hoffman F., Opitz S., Riemenschneider J., "*Validation of Active Twist Modeling Based on Whirl Tower Tests*", 65th American Helicopter Society Forum, Grapevine, Texax, May 27-29, 2009
[13] Allongue M., Krysinski T., "*Validation of a New General Aerospatiale Aeroelastic Rotor Model through the Wind Tunnel and Flight Test Data*", 46th American Helicopter Society Forum, Washington D.C., May 1990
[14] Arnaud G., Beaumier P., "*Validation of R85/METAR on the Puma RAE Flight Tests*", 18th European Rotorcraft Forum, Avignon, France, September 1992
[15] Michéa B., Desopper A., Costes M., *"Aerodynamic Rotor Loads Prediction Method with Free Wake for Low Speed Descent Flight*", 18th European Rotorcraft Forum, Avignon, France, September 1992
[16] Rahier G., Delrieux Y., *"Improvement of Helicopter Rotor Blade-Vortex Interaction Noise Prediction using a Rotor Wake Roll-Up Model"*, 16th AIAA Aeroacoustic Conference, Munich, Germany, June 1995
[17] Spiegel P., Rahier G., Michéa B., *"Blade-Vortex Interaction Noise: Prediction and Comparison with Flight and Wind-Tunnel Tests"*, 18th European Rotorcraft Forum, Avignon, France, September 1992
[18] Spiegel P., Rahier G., *"Theoretical Study and Prediction of BVI Noise including Close Interactions"*, AHS Technical Specialists Meeting on Rotorcraft Acoustics and Fluid Mechanics, Philadelphia, PA, October 1991
[19] Le Pape A., *"Numerical Aerodynamic Optimization of Helicopter Rotors: Multi-Objective Optimization in Hover and Forward Flight Conditions"*, 31st European Rotorcraft Forum, Firenze, Italy, September 2005
[20] Vanderplaats G.N., *"CONMIN: a FORTAN rogram for Constrained Function Minimization"*, NASA TMX 62282, 1973
[21] Rashhed K., "*GADO: a Genetic Algorithm for Continuous Design Optimization*", Phd Thesis, Rutgers, State University of New Jersey, January 1998
[22] Wierach P., Riemenschneider J., Opitz S., Hoffman F.,"*Experimental Investigation of an Active Twist Model Rotor under Centrifugal Loads*", 33rd European Rotorcraft Forum, Kazan, Russia, September 2007
[23] Delrieux Y., Le Pape A., Leconte P., Crozier P., Gimonet B., Mercier des Rochettes H., "*Wind Tunnel Assessment of the Concept of Active Flaps on a Helicopter Rotor Model",* 63rd American Helicopter Society Forum, Virginia Beach (VA), USA, May 1-3, 2007